Published in final edited form as:
IEEE Trans Ultrason Ferroelectr Freq Control. 2014 October ; 61(10): 1619–1626. doi:10.1109/TUFFC.2014.006316.

Removal of Residual Nuclei Following a Cavitation Event using Low-Amplitude Ultrasound

Alexander P. Duryea[1], **Charles A. Cain**[1], **Hedieh A. Tamaddoni**[1], **William W. Roberts**[1,2], and **Timothy L. Hall**[1]

[1]Department of Biomedical Engineering, University of Michigan, Ann Arbor, MI, USA

[2]Department of Urology, University of Michigan, Ann Arbor, MI, USA

Abstract

Microscopic residual bubble nuclei can persist on the order of 1 second following a cavitation event. These bubbles can limit the efficacy of ultrasound therapies such as shock wave lithotripsy and histotripsy, as they attenuate pulses that arrive subsequent to their formation and seed repetitive cavitation activity at a discrete set of sites (cavitation memory). Here, we explore a strategy for the removal of these residual bubbles following a cavitation event, using low amplitude ultrasound pulses to stimulate bubble coalescence. All experiments were conducted in degassed water and monitored using high speed photography. In each case, a 2 MHz histotripsy transducer was used to initiate cavitation activity (a cavitational bubble cloud), the collapse of which generated a population of residual bubble nuclei. This residual nuclei population was then sonicated using a 1 ms pulse from a separate 500 kHz transducer, which we term the 'bubble removal pulse.' Bubble removal pulse amplitudes ranging from 0 to 1.7 MPa were tested, and the backlit area of shadow from bubbles remaining in the field following bubble removal was calculated to quantify efficacy. It was found that an ideal amplitude range exists (roughly 180 – 570 kPa) in which bubble removal pulses stimulate the aggregation and subsequent coalescence of residual bubble nuclei, effectively removing them from the field. Further optimization of bubble removal pulse sequences stands to provide an adjunct to cavitation-based ultrasound therapies such as shock wave lithotripsy and histotripsy, mitigating the effects of residual bubble nuclei that currently limit their efficacy.

INTRODUCTION

Collapse of the primary cavitation bubbles generated by a high intensity acoustic pulse can produce an extensive population of residual bubble nuclei [1–9]. A single primary bubble can give rise to dozens of residual daughters, as its collapse is typically accompanied by fission into numerous remnant fragments [1, 4, 7, 8]. The resulting daughter bubbles are microscopic in size (<10 μm) [10, 11] and can persist for tens of milliseconds [6, 12] or even full seconds [3, 7, 8, 13], depending on the conditions under which they were generated. If

DISCOLOSURE

C.A. Cain, W.W. Roberts, and T.L. Hall have financial interests and/or other relationships with HistoSonics, Inc., which has licensed intellectual property related to this manuscript.

additional acoustic pulses are applied prior to the dissolution of these residual bubbles, they can serve as nuclei to seed subsequent cavitation activity [1–3, 5, 6]. As such, residual bubble nuclei impart a cavitation memory to their host medium, influencing the threshold, extent, and distribution of ensuing cavitation events [9, 14–18].

Residual bubble nuclei that persist from one pulse to the next can limit the efficiency of cavitation-based ultrasound therapies. In shock wave lithotripsy (SWL) the efficacy of stone comminution is highly dependent on the rate of shock wave (SW) delivery, with testing both *in-vitro* [16, 19–22] and *in-vivo* [23] demonstrating a decrease in per-shock fragmentation efficiency with increasing shock rate. This is a result of extensive cavitation generated along the SW propagation path, the collapse of which produces a large population of residual nuclei [7, 8]. When a SW propagates through a medium containing these residual bubbles, the tensile component of the waveform causes them to expand—a process that selectively attenuates the SW's negative tail and reduces the energy that ultimately reaches the stone [10, 16, 18, 24]. At high shock rates residual nuclei have less time to passively dissolve between successive SWs, leading to more severe attenuation of the negative phase and compromised comminution efficacy.

Rate-dependent efficiency has also been observed in histotripsy therapy [9], which utilizes high-intensity (peak negative pressure >10 MPa), extremely short (<50 μs) ultrasound pulses at low duty cycles (<1%) to control acoustic cavitation for the mechanical fractionation of soft tissue [25–27]. In this case it is cavitation memory—i.e., the repetitive initiation of cavitation at a discrete set of sites within the focal zone—that is the primary source of less efficient lesion formation at high pulse repetition frequencies [9]. Residual nuclei that persist between histotripsy pulses can seed this cavitation memory effect, resulting in inhomogeneous tissue fractionation and requiring an excess number of pulses to achieve complete homogenization of the targeted volume. It has been demonstrated that by increasing the time between successive histotripsy pulses such that remnant nuclei can more completely dissolve, cavitation bubbles are generated at a more randomized set of sites within the focal zone and complete homogenization is achieved using fewer pulses [9].

The ability to manipulate residual bubble nuclei following primary cavitation collapse would be of great benefit to ultrasound therapies such as SWL and histotripsy. In the present study, we explore a strategy for the active removal of these residual bubbles, using low amplitude ultrasound bursts to stimulate nuclei coalescence. It has been well documented that when microscopic bubbles are exposed to a sound field, forces develop that can promote either their aggregation or dispersion [28–34]. These, collectively referred to as the Bjerknes forces, offer a means of manipulating the population of residual bubble nuclei following cavitation collapse. Here we investigate acoustic sequences that permit the Bjerknes forces to act in concert to stimulate the aggregation and subsequent coalescence of cavitation nuclei —effectively removing them from the field. It is our hope that an optimized form of these bubble removal sequences will provide an adjunct to cavitation-based ultrasound therapies that suffer from the ill-effects of residual bubble nuclei.

METHODS

A. Experimental Setup

The experimental setup used to study the effect of low-amplitude acoustic bursts on residual bubble nuclei is displayed in Fig. 1. All experiments were conducted in deionized water degased to physiologically relevant levels (dissolved oxygen content of 7.3 ± 0.6 mg/L at 20.3 ± 3.5 °C (mean ± SD), corresponding to 79 ± 1% of saturation); this mimics the dissolved gas content of human urine, for example [35–37]. Each experiment was monitored using a Photron Fastcam SA1.1 high speed camera (Photron USA Inc., San Diego, CA) at a frame rate of 20 kfps and exposure time of 49 μs. A 10X super-long working distance microscope objective (T Plan SLWD 10X/0.20, Nikon Instruments Inc., Tokyo, Japan) coupled to a 70 mm macro lens (Sigma 70 mm 1:2:8 DG Macro, Sigma Corporation of America, Ronkonkoma, NY) provided the optical power to resolve the microscopic residual nuclei of interest in this study. The theoretical resolution limit of this optical setup is 1.3 μm, while the theoretical depth of field is 18.3 μm. A large area, high power LED light source (BXRA-50C9000, Bridgelux Inc., Livermore, CA) was used to backlight the experiments such that bubbles generated in the field were visible as dark shadows on the optical images.

A 2 MHz histotripsy transducer constructed in-house was used to initiate primary cavitation activity (a cavitational bubble cloud). It consisted of eight PZT-4 disc elements (Steiner & Martins Inc., Miami, FL), measuring 10 mm in diameter and 1 mm in thickness. Water-tight modules designed to hold individual elements were fabricated from Accura 60 plastic (3D Systems Inc., Rock Hill, SC) using a stereolithography machine. The front face of each module contained an Accura 60 acoustic lens with a focal length of 20 mm; PZT-4 elements were matched to this lens using an epoxy (1C-LV Hysol, Loctite Corporation, Rocky Hill, CT) filled 100 mesh copper screen (McMaster-Carr, Aurora, OH) to achieve the proper thickness and impedance. The eight individual histotripsy modules were aligned confocally in a spherical arrangement using a plastic scaffold, also fabricated via stereolithography from Accura 60. This scaffold doubled as the water tank for the experiments, and had optical windows in the front and rear to permit the use of backlit high speed photography. The spherical geometry of this transducer produced a highly confined focal zone, with the −6-dB beamwidths measuring approximately 500 μm in both the lateral and axial dimensions. These measurements were conducted at a pressure amplitude of 6 MPa (linear regime) using a fiber optic hydrophone with a 100 μm diameter sensing tip [38]. The histotripsy transducer was driven using a pulse amplifier developed in our lab, which was designed to produce very short intense bursts. More details regarding the acoustic output generated by this setup are provided in the subsequent section.

A separate 500 kHz transducer—which we denote as the bubble removal module—was used to sonicate residual cavitation nuclei produced by collapse of the histotripsy bubble cloud. Similar to the histotripsy modules, this transducer was constructed in-house using a stereolithography-fabricated Accura 60 housing and acoustic lens, in this case having a focal length of 25 mm. Two 1 MHz Pz36 disc elements (Ferroperm Piezoceramics A/S, Kvistgaard, Denmark) measuring 20 mm in diameter and 1.6 mm in thickness were stacked and driven in unison to produce a 500 kHz equivalent source. The front face of this Pz36

stack was mated directly to the Accura 60 acoustic lens using epoxy adhesive (Hysol E-120 HP, Loctite Corporation, Rocky Hill, CT); a copper screen matching layer was not utilized in this case due to the low acoustic impedance of Pz36 (specified at 14 MRayl by the manufacturer). The bubble removal module was held within the same spherical scaffold used to position the histotripsy modules and aligned coincident with their geometric focus (Fig. 1). It produced an acoustic field with −6-dB beamwidths measuring 4.3 mm in the lateral dimension and exceeding 20 mm in the axial; as such, the bubble removal field was much broader than the 500 μm wide focal zone of the histotripsy transducer, encompassing the full extent of histotripsy-induced cavitation bubbles. These field scans were performed at a pressure amplitude of 500 kPa (linear regime) using an HNR-0500 needle hydrophone (Onda Corporation, Sunnyvale, CA). The bubble removal module was driven using a 500 kHz sinusoid from an ENI AP400B controllable power amplifier (Electronic Navigation Industries Inc., Rochester, NY); further details on the acoustic output are presented in the subsequent section.

B. Acoustic Pulse Sequence

Three general types of acoustic pulses were utilized in this study, as represented in Fig. 2(a) –Fig. 2(c): (1) Histotripsy pulses generated by the 2 MHz histotripsy transducer were used to initiate cavitation activity in the form of a cavitational bubble cloud; (2) Bubble removal pulses produced by the 500 kHz bubble removal module were used to sonicate residual bubble nuclei following primary cavitation collapse, stimulating their coalescence and de facto removal from the field; (3) An interrogation pulse, also delivered from the 500 kHz bubble removal module, was used to probe the field for the presence of residual nuclei following bubble removal. This pulse caused remaining microscopic nuclei to expand and be more easily detected via high speed imaging. The overall timing of this pulse scheme is summarized in Fig. 2(d), with specifics provided henceforth.

The initiation of primary cavitation activity in this study was achieved using a train of five histotripsy pulses delivered at a pulse repetition frequency (PRF) of 1 kHz. Histotripsy pulses were very short (approximately 2 μs) and intense. The acoustic output from a single histotripsy module is displayed in Fig. 2(a), measured using the same fiber optic hydrophone used to perform histotripsy field scans. Due to the sparse and spherical distribution of the modules that compose the histotripsy transducer, there is minimal superposition of individual waveforms until they reach the geometric focal location; as such, we estimate the output of the histotripsy transducer as the linear sum of the outputs from the eight individual modules [39]—suggesting a peak negative pressure of approximately 40 MPa. This overall output exceeds the intrinsic cavitation threshold in water [39], permitting the histotripsy transducer to initiate a cavitational bubble cloud with each pulse. A train of five histotripsy pulses in rapid succession was utilized to maximize the extent of cavitation. Similar to the bubble proliferation phenomenon observed in SWL [7, 8], this arrangement of histotripsy pulses was empirically determined to enhance cavitation activity as residual daughter bubbles persisting between pulses seeded additional sites for cavitation inception.

Following collapse of the final histotripsy-induced bubble cloud, residual cavitation nuclei were sonicated with a 1 ms long bubble removal pulse to stimulate their removal from the

field via bubble coalescence. A partial segment of a representative bubble removal pulse is displayed in Fig. 2(b), acquired using the same HNR-0500 needle hydrophone used to perform bubble removal module field scans. All bubble removal pulses had a center frequency of 500 kHz and were applied at a delay of 500 μs following the final histotripsy pulse; the later allowed the histotripsy bubble cloud to collapse and produce residual nuclei in an unimpeded manner. To investigate the influence of acoustic pulse amplitude on the bubble removal process, bubble removal pulse amplitudes of 0, 80, 150, 180, 230, 310, 400, 570, 750, 1100, and 1700 kPa were tested. As the bubble removal pulses were observed to have some amplitude variation across their 1 ms duration (~10%), these reported values represent the mean amplitude over all 500 cycles of the pulse. It should be noted that the bubble removal pulse parameters utilized in this study have not yet been optimized, and were selected following a very coarse parametric investigation. As such, these pulses are intended solely for introducing the concept of removing residual nuclei following a cavitation event.

The presence of residual nuclei remaining in the field following the bubble removal pulse was probed for using a second, much shorter, pulse from the 500 kHz bubble removal module, which we denote as the interrogation pulse. In a separate set of experiments not reported in this manuscript, the individual residual bubble nuclei produced by the 2 MHz histotripsy transducer were observed to fall in a tight size distribution with a mean diameter of approximately 6 μm. Although this is larger than the 1.3 μm theoretical resolution limit of our optical setup, these individual microscopic residual nuclei may fall out of the depth of field imaging plane (estimated at 18 μm) and therefore be difficult to detect and quantify. For this reason, the interrogation pulse was used to expand any bubble nuclei remaining in the field such that they could be more easily detected via high speed imaging. Fig. 2(c) displays the interrogation pulse waveform used for all experiments in this study, as calibrated by the HNR-0500 needle hydrophone. In all cases, a 10 cycle pulse with amplitude of 2.5 MPa was used to interrogate the field at 500 μs following the completion of the bubble removal pulse. This interrogation pulse was found not to initiate any cavitation bubbles independently (i.e., when not preceded by the generation of a population of cavitation bubble nuclei).

C. Quantification of Bubble Removal Pulse Efficacy

To quantify the efficacy of bubble removal, the backlit area of shadow of remnant nuclei expanded by the interrogation pulse was calculated. The entire duration of each pulse sequence was imaged using high speed photography at 20 kfps, and it was empirically determined that the 120th frame in the image sequence corresponded to the time point of maximal bubble expansion induced by the interrogation pulse. The backlit area of bubble shadow in this frame was calculated for all experiments using Matlab (MathWorks Inc., Natick, MA) to sum the pixels that resided below a threshold value. Ten trials were performed at each bubble removal pulse amplitude tested.

RESULTS

Representative image sequences showing the activity of residual bubble nuclei over the course of the bubble removal and interrogation pulses are displayed for select cases in Fig. 3, while the backlit area of shadow from bubbles expanded by the interrogation pulse is quantified for all cases in Fig. 4. Collapse of the final histotripsy bubble cloud was observed to produce an extensive set of microscopic residual bubble nuclei. In the control case (bubble removal pulse amplitude set to 0) these residual bubbles persisted over the entirety of the 1 ms bubble removal pulse duration, gradually dispersing with time (Fig. 3, row 1). Applying the interrogation pulse to this bubble population facilitated its visualization with the high speed camera (Fig. 3, row 1, column 7); the average interrogated bubble shadow area resulting from the ten control trials was used to normalize all values presented in Fig. 4.

At the lowest bubble removal pulse amplitudes of 80 and 150 kPa minimal bubble coalescence was observed. Instead, dispersion of the residual bubbles was stimulated, with a portion of the nuclei population migrating in the direction of bubble removal pulse propagation. This phenomenon can be observed in the second row of images displayed in Fig. 3. Correspondingly, the backlit area of shadow of interrogated bubbles did not show a statistically significant deviation from the control case at these amplitudes (*t-test*, $P > 0.42$), with respective normalized values (mean ± SD) of 0.96 ± 0.11 and 1.01 ± 0.08 (Fig. 4).

Intermediate bubble removal pulse amplitudes of 180 – 570 kPa were found to stimulate the aggregation and subsequent coalescence of residual bubble nuclei, as can be observed in the third row of Fig. 3. In these cases the residual bubble population was consolidated from a very large number of remnant nuclei down to a countably small number of residual bubbles. Correspondingly, a statistically significant reduction in the interrogated bubble shadow area relative to control (Fig. 4) was observed for all bubble removal pulse amplitudes in this range (*t-test*, $P < 1E\text{-}10$). The extent of the coalescence process was observed to become more pronounced as the bubble removal pulse amplitude was increased from 180 to 570 kPa; this translated to a progressive reduction in interrogated bubble shadow area (*t-test*, $P < 0.001$) until reaching a minimum in the vicinity of 310 – 570 kPa. Specifically, bubble removal pulses with amplitudes of 180, 230, and 310 kPa were found to produce normalized interrogated bubble shadow areas of 0.53 ± 0.05, 0.25 ± 0.08, and 0.12 ± 0.06, respectively. No further reduction was observed for bubble removal pulses greater than 310 kPa, with amplitudes of 400 and 570 kPa producing normalized interrogated bubble shadow areas of 0.14 ± 0.04 and 0.14 ± 0.05 (*t-test*, $P > 0.50$).

Further increasing the bubble removal pulse amplitude above 570 kPa did not maintain or enhance the extent of bubble coalescence; rather, the highest tested amplitudes of 750, 1100, and 1700 kPa showed a reduction in the efficacy of the coalescence process. While pulses in this amplitude range continued to stimulate the aggregation of residual bubble nuclei, coalescence was compromised by the fact that these higher amplitude pulses re-excited residual bubbles and caused them to undergo violent cavitation—the collapse of which produced additional residual daughter nuclei (Fig. 3, row 4). As a result, interrogated bubble shadow area (Fig. 4) was observed to increase with increasing bubble removal pulse amplitude from 750 to 1700 kPa (*t-test*, $P < 0.001$), with removal pulse amplitudes of 750,

1100, and 1700 kPa resulting in normalized values of 0.26 ± 0.05, 0.48 ± 0.05, and 0.85 ± 0.29, respectively. The later result at the highest tested bubble removal pulse amplitude of 1700 kPa did not deviate significantly from the control case (*t-test*, P = 0.14).

DISCUSSION

This study investigates a unique strategy for mitigating the effects of residual bubble nuclei produced by cavitation collapse, using low-amplitude acoustic bursts to stimulate their removal from the field via bubble coalescence. It was shown that these bubble removal pulses produce three distinct regimes of remnant nuclei behavior depending on the pulse amplitude utilized: (1) When sonicated at low amplitudes (150 kPa and below), residual bubbles experience minimal coalescence, although some dispersion of the nuclei is observed; (2) At intermediate amplitudes (180 – 570 kPa), the aggregation and subsequent coalescence of nuclei is stimulated—effectively removing them from the field; (3) High amplitudes (750 kPa and above) show a decrease in the efficacy of coalescence, resulting from the re-excitation of remnant nuclei and production of additional residual daughter bubbles.

We hypothesize that the primary and secondary Bjerknes forces are the major facilitators of the bubble coalescence phenomenon of interest in this study. Briefly, bubbles oscillating in an acoustic field will experience two major sets of forces [28–34, 40, 41]. The first, the primary Bjerknes force, describes the effect of the acoustic field on individual bubbles [31–33, 40, 41]. Theory dictates that bubbles smaller than the resonant size of the sonication frequency will be stimulated to migrate up the pressure gradient and congregate at antinodes, while those larger than the resonant size of the sonication frequency are stimulated to migrate down the pressure gradient and congregate at nodes. The second major force on acoustically driven bubbles, the secondary Bjerknes force, describes the effect of neighboring bubbles on one another [31, 32, 34, 41]. In this case theory suggests that bubbles that are of similar size such that their phase difference of oscillation is less than $\pi/2$ will experience an attractive force. Conversely, bubbles that are very different in size such that their phase difference of oscillation is greater than $\pi/2$ will experience a repulsive force. Overall, the Bjerknes forces can manifest in the aggregation or dispersion of acoustically driven bubbles, depending on the bubble size distribution relative to the sonication frequency. This fact has been observed experimentally in numerous studies [31–34, 40, 42, 43], including more recent work in the field of ultrasound contrast agent imaging [44–47].

In the present study, 500 kHz bubble removal pulses delivered at intermediate amplitudes were found to stimulate the most effective coalescence of residual bubble nuclei. Based on the Minnaert formula [48], the frequency of 500 kHz corresponds to an equilibrium bubble diameter of 12 μm. Our high speed imaging suggests that the remnant nuclei produced by collapse of the histotripsy bubble cloud were smaller than this resonant size, falling in a very tight size distribution with equilibrium diameter of approximately 6 μm. As such, it is likely that the primary and secondary Bjerknes forces act in concert to stimulate the bubble coalescence observed in this study: the primary force stimulates the migration of residual bubble nuclei up the pressure gradient toward the antinode of the bubble removal transducer, while the secondary force facilitates the attraction of individual bubbles to one another.

Ultimately, this synergistic manipulation of residual nuclei manifests in their aggregation and subsequent coalescence. Our future work regarding the optimization of the coalescence process will aim to verify this hypothesis through both experimental and theoretical investigations of the effect of bubble removal pulse frequency.

The fact that different regimes of bubble nuclei behavior were observed as the bubble removal pulse amplitude was increased suggests that the relative contributions of the primary and secondary Bjerknes forces have an amplitude dependence. Indeed, it has been previously documented that the secondary Bjerknes force increases with intensity more significantly than the primary [49–51]. This suggests that the efficacious aggregation and coalescence of residual nuclei observed at intermediate bubble removal pulse amplitudes has a strong dependence on the magnitude of this secondary force. A similar conclusion was presented by Hatanaka, *et al*. [49], who determined that bubble clustering observed at excessive ultrasonic intensity is predominantly due to the secondary Bjerknes force. This theory is consistent with the fact that, at the lower bubble removal pulse amplitudes tested in this study, minimal coalescence was observed. Instead, prominent dispersion of residual nuclei occurred. It is possible that these residual bubbles grew to sizes greater than the 12 μm resonant size of the isonification frequency, either by some limited degree of coalescence or rectified diffusion, at which point they migrated down the pressure gradient of the bubble removal sound field. Such behavior would give rise to the distribution of nuclei depicted in the second row of Fig. 3. As the bubble removal pulse amplitude was increased and the secondary Bjerknes force became more dominant, this behavior was likely offset by the stronger degree of inter-bubble attraction. Quantitative simulations are currently being explored to better characterize the relative contributions of these forces for bubble removal.

The ability to actively remove residual bubble nuclei from the field has the potential to markedly enhance the efficacy of cavitation-based ultrasound therapies. In SWL the efficiency of stone comminution has been documented to decrease as the rate of SW application increases [16, 19–23]—a phenomenon attributed to remnant cavitation nuclei that persist from one SW to the next. When SWs propagate through a field containing these residuals, they experience a selective attenuation of their negative phase [10, 16, 18, 24] that compromises fragmentation of the stone. A similar rate dependent efficiency is observed in histotripsy treatment of soft tissue, albeit due to cavitation memory rather than direct attenuation of the acoustic waveform [9]. Residual bubble nuclei that persist between histotripsy pulses can seed repetitive cavitation at a discrete set of sites within the focal volume, leading to inhomogeneous tissue fractionation and requiring an excess number of pulses to achieve complete homogenization of the targeted volume. Increasing the time between successive pulses such that remnant nuclei can dissolve more completely has been shown to enhance the efficiency of histotripsy treatment, permitting cavitation bubbles to nucleate at a more randomized set of sites within the focal zone [9]. Clearly, the strategic manipulation of residual bubble nuclei following the collapse of primary acoustic cavitation could be of great benefit in both SWL and histotripsy. It is our hope that further optimization of bubble removal pulse sequences will provide an adjunct to these therapies, enabling them to achieve levels of efficiency not previously possible due to the effects of residual bubbles.

CONCLUSION

In this study it was demonstrated that acoustic pulses can actively remove residual cavitation bubble nuclei from the field by stimulating their aggregation and subsequent coalescence. We hypothesize that the primary and secondary Bjerknes forces act in concert to facilitate this process, with the secondary force playing a more dominant role. Application of bubble removal pulse sequences to cavitation-based ultrasound therapies such as SWL and histotripsy will likely mitigate the rate dependent limitations that stem from the persistence of residual bubbles. Our future work will focus on the optimization of these bubble removal sequences, as well as their implementation in SWL and histotripsy treatments.

Supplementary Material

Refer to Web version on PubMed Central for supplementary material.

Acknowledgments

Research reported in this publication was supported by The National Institute of Diabetes and Digestive and Kidney Diseases of the National Institutes of Health under award number R01DK091267. The content is solely the responsibility of the authors and does not necessarily represent the official views of the National Institutes of Health.

REFERENCES

1. Flynn HG, Church CC. A mechanism for the generation of cavitation maxima by pulsed ultrasound. J Acoust Soc Am. 1984 Aug.76:505–512. [PubMed: 6481000]
2. Fowlkes JB, Crum LA. Cavitation threshold measurements for microsecond length pulses of ultrasound. The Journal of the Acoustical Society of America. 1988; 83:2190–2201. [PubMed: 3411016]
3. Huber P, Jochle K, Debus J. Influence of shock wave pressure amplitude and pulse repetition frequency on the lifespan, size and number of transient cavities in the field of an electromagnetic lithotripter. Phys Med Biol. 1998 Oct.43:3113–3128. [PubMed: 9814538]
4. Brennen CE. Fission of collapsing cavitation bubbles. Journal of Fluid Mechanics. 2002; 472:153–166.
5. Arora M, Junge L, Ohl CD. Cavitation cluster dynamics in shock-wave lithotripsy: part 1. Free field. Ultrasound Med Biol. 2005 Jun.31:827–839. [PubMed: 15936498]
6. Xu Z, Hall TL, Fowlkes JB, Cain CA. Optical and acoustic monitoring of bubble cloud dynamics at a tissue-fluid interface in ultrasound tissue erosion. The Journal of the Acoustical Society of America. 2007; 121:2421–2430. [PubMed: 17471753]
7. Pishchalnikov, YA.; McAteer, JA.; Pishchalnikova, IV.; Williams, JC.; Bailey, MR.; Sapozhnikov, OA. Bubble proliferation in shock wave lithotripsy occurs during inertial collapse; 18th International Symposium on Nonlinear Acoustics; 2008. p. 460-463.
8. Pishchalnikov YA, Williams JC, McAteer JA. Bubble proliferation in the cavitation field of a shock wave lithotripter. J Acoust Soc Am. 2011 Aug.130:EL87–EL93. [PubMed: 21877776]
9. Wang TY, Xu Z, Hall TL, Fowlkes JB, Cain CA. An efficient treatment strategy for histotripsy by removing cavitation memory. Ultrasound Med Biol. 2012 May.38:753–766. [PubMed: 22402025]
10. Pishchalnikov YA, McAteer JA, Williams JC Jr. Effect of firing rate on the performance of shock wave lithotriptors. BJU Int. 2008 Dec.102:1681–1686. [PubMed: 18710450]
11. Mettin R, Akhatov I, Parlitz U, Ohl CD, Lauterborn W. Bjerknes forces between small cavitation bubbles in a strong acoustic field. Physical Review E. 56:2924–2931.

12. Chen WS, Matula TJ, Crum LA. The disappearance of ultrasound contrast bubbles: observations of bubble dissolution and cavitation nucleation. Ultrasound Med Biol. 2002 Jun.28:793–803. [PubMed: 12113792]
13. Epstein PS, Plesset MS. On the stability of gas bubbles in liquid-gas solutions. The Journal of Chemical Physics. 1950; 18:1505–1509.
14. Arora M, Ohl CD, Lohse D. Effect of nuclei concentration on cavitation cluster dynamics. J Acoust Soc Am. 2007 Jun.121:3432–3436. [PubMed: 17552694]
15. Yavas O, Leiderer P, Park HK, Grigoropoulos CP, Poon CC, Tam AC. Enhanced acoustic cavitation following laser-induced bubble formation: Long-term memory effect. Physical Review Letters. 72:2021–2024. [PubMed: 10055768]
16. Pishchalnikov YA, McAteer JA, Williams JC Jr, Pishchalnikova IV, Vonderhaar RJ. Why stones break better at slow shockwave rates than at fast rates: in vitro study with a research electrohydraulic lithotripter. J Endourol. 2006 Aug.20:537–541. [PubMed: 16903810]
17. Sapozhnikov OA, Khokhlova VA, Bailey MR, Williams JC Jr, McAteer JA, Cleveland RO, et al. Effect of overpressure and pulse repetition frequency on cavitation in shock wave lithotripsy. J Acoust Soc Am. 2002 Sep.112:1183–1195. [PubMed: 12243163]
18. Pishchalnikov YA, Sapozhnikov OA, Bailey MR, Pishchalnikova IV, Williams JC, McAteer JA. Cavitation selectively reduces the negative-pressure phase of lithotripter shock pulses. Acoust Res Lett Online. 2005 Nov 3.6:280–286. [PubMed: 19756170]
19. Vallancien G, Munoz R, Borghi M, Veillon B, Brisset JM, Daudon M. Relationship between the frequency of piezoelectric shock waves and the quality of renal stone fragmentation. In vitro study and clinical implications. Eur Urol. 1989; 16:41–44. [PubMed: 2714316]
20. Wiksell H, Kinn AC. Implications of cavitation phenomena for shot intervals in extracorporeal shock wave lithotripsy. Br J Urol. 1995 Jun.75:720–723. [PubMed: 7613826]
21. Greenstein A, Matzkin H. Does the rate of extracorporeal shock wave delivery affect stone fragmentation? Urology. 1999; 54:430–432. [PubMed: 10475348]
22. Weir MJ, Tariq N, Honey RJ. Shockwave frequency affects fragmentation in a kidney stone model. J Endourol. 2000 Sep.14:547–550. [PubMed: 11030533]
23. Paterson RF, Lifshitz DA, Lingeman JE, Evan AP, Connors BA, Fineberg NS, et al. Stone fragmentation during shock wave lithotripsy is improved by slowing the shock wave rate: studies with a new animal model. J Urol. 2002 Nov.168:2211–2215. [PubMed: 12394761]
24. Pishchalnikov, YA.; McAteer, JA.; Bailey, MR.; Pishchalnikova, IV.; Williams, JC.; Evan, AP. Acoustic shielding by cavitation bubbles in shock wave lithotripsy (SWL); 17th International Symposium on Nonlinear Acoustics; 2005. p. 319-322.
25. Xu Z, Ludomirsky A, Eun LY, Hall TL, Tran BC, Fowlkes JB, et al. Controlled ultrasound tissue erosion. IEEE Trans Ultrason Ferroelectr Freq Control. 2004 Jun.51:726–736. [PubMed: 15244286]
26. Parsons JE, Cain CA, Abrams GD, Fowlkes JB. Pulsed cavitational ultrasound therapy for controlled tissue homogenization. Ultrasound Med Biol. 2006 Jan.32:115–129. [PubMed: 16364803]
27. Roberts WW, Hall TL, Ives K, Wolf JS Jr, Fowlkes JB, Cain CA. Pulsed cavitational ultrasound: a noninvasive technology for controlled tissue ablation (histotripsy) in the rabbit kidney. J Urol. 2006 Feb.175:734–738. [PubMed: 16407041]
28. Bjerknes V. Fields of Force. 1906
29. Bjerknes V. Die Kraftfelder. 1909
30. Kornfeld M, Suvorov L. On the destructive action of cavitation. Journal of Applied Physics. 1944; 15:495–506.
31. Blake FG. Bjerknes Forces in Stationary Sound Fields. The Journal of the Acoustical Society of America. 1949; 21:551–551.
32. Neppiras EA. Subharmonic and Other Low-Frequency Emission from Bubbles in Sound-Irradiated Liquids. The Journal of the Acoustical Society of America. 1969; 46:587–601.
33. Crum LA, Eller AI. Motion of Bubbles in a Stationary Sound Field. The Journal of the Acoustical Society of America. 1970; 48:181–189.

34. Crum LA. Bjerknes forces on bubbles in a stationary sound field. The Journal of the Acoustical Society of America. 1975; 57:1363–1370.
35. Chaigneau M, Le Moan G. On the composition of gas dissolved in human urine. C R Acad Sci Hebd Seances Acad Sci D. 1968 Nov 25.267:1893–1895. [PubMed: 4973654]
36. Fowlkes JB, Carson PL, Chiang EH, Rubin JM. Acoustic generation of bubbles in excised canine urinary bladders. J Acoust Soc Am. 1991 Jun.89:2740–2744. [PubMed: 1918622]
37. Hwang EY, Fowlkes JB, Carson PL. Variables controlling contrast generation in a urinary bladder model. J Acoust Soc Am. 1998 Jun.103:3706–3716. [PubMed: 9637051]
38. Parsons JE, Cain CA, Fowlkes JB. Cost-effective assembly of a basic fiber-optic hydrophone for measurement of high-amplitude therapeutic ultrasound fields. J Acoust Soc Am. 2006 Mar. 119:1432–1440. [PubMed: 16583887]
39. Maxwell AD, Cain CA, Hall TL, Fowlkes JB, Xu Z. Probability of Cavitation for Single Ultrasound Pulses Applied to Tissues and Tissue-Mimicking Materials. Ultrasound in Medicine & Biology. 2013; 39:449–465. 3//. [PubMed: 23380152]
40. Crum LA. The motion of bubbles in a stationary sound field. The Journal of the Acoustical Society of America. 1969; 46:1411.
41. Leighton, TG. The Acoustic Bubble. San Diego, CA: Academic Press Inc; 1997.
42. Goldman DE, Ringo GR. Determination of Pressure Nodes in Liquids. The Journal of the Acoustical Society of America. 1949; 21:270–270.
43. Nyborg WL, Hughes DE. Bubble annihilation in cavitation streamers. The Journal of the Acoustical Society of America. 1968; 42:891–894.
44. Dayton P, Klibanov A, Brandenburger G, Ferrara K. Acoustic radiation force in vivo: a mechanism to assist targeting of microbubbles. Ultrasound Med Biol. 1999 Oct.25:1195–1201. [PubMed: 10576262]
45. Dayton PA, Allen JS, Ferrara KW. The magnitude of radiation force on ultrasound contrast agents. J Acoust Soc Am. 2002 Nov.112:2183–2192. [PubMed: 12430830]
46. Zhao S, Borden M, Bloch SH, Kruse D, Ferrara KW, Dayton PA. Radiation-force assisted targeting facilitates ultrasonic molecular imaging. Mol Imaging. 2004 Jul.3:135–148. [PubMed: 15530249]
47. Ferrara K, Pollard R, Borden M. Ultrasound microbubble contrast agents: fundamentals and application to gene and drug delivery. Annu Rev Biomed Eng. 2007; 9:415–447. [PubMed: 17651012]
48. Minnaert M. XVI. On musical air-bubbles and the sounds of running water. Philosophical Magazine Series 7. 1933; 16:235–248.
49. Hatanaka S, Yasui K, Kozuka T, Tuziuti T, Mitome H. Influence of bubble clustering on multibubble sonoluminescence. Ultrasonics. 2002 May.40:655–660. [PubMed: 12160020]
50. Lauterborn W, Kurz T, Mettin R, Ohl CD. Experimental and theoretical bubble dynamics. Adv. Chem. Phys. 1999; 110:295–380.
51. Mettin R, Luther S, Ohl CD, Lauterborn W. Acoustic cavitation structures and simulations by a particle model. Ultrasonics Sonochemistry. 1999; 6:25–29. [PubMed: 11233935]

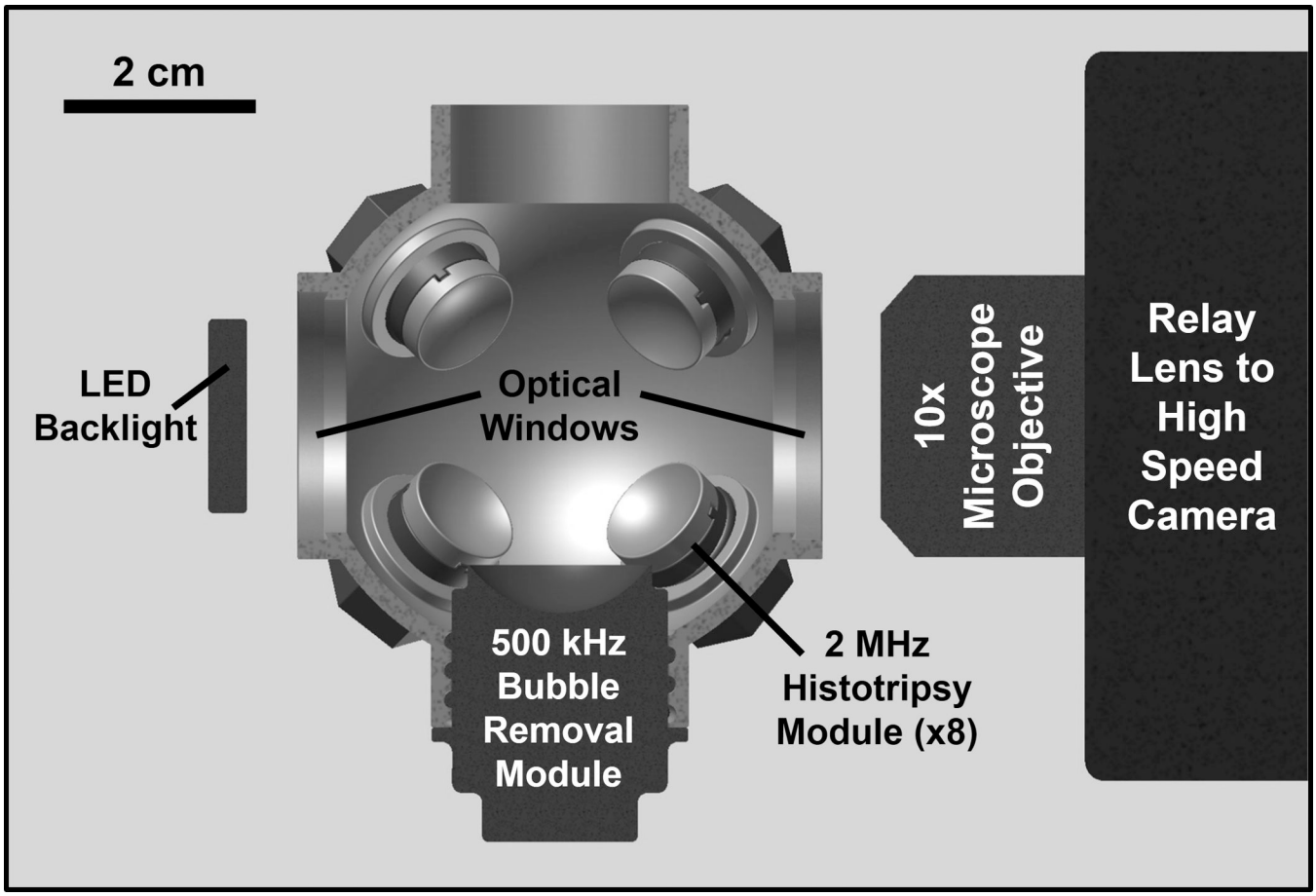

Fig. 1.

Half-section view of the experimental setup used to study effects of low-amplitude acoustic bursts on residual cavitation bubble nuclei. Primary cavitation was initiated by an array of eight 2 MHz histotripsy modules arranged in a spherical pattern, while bubble removal pulses were delivered from a separate 500 kHz module aligned confocally (see text for details on module construction). All transducer modules were held within an Accura 60 plastic scaffold that also served as the water tank for the experiments. Optical windows in the front and rear of the scaffold allowed for the use of backlit high speed photography to monitor the bubble removal process.

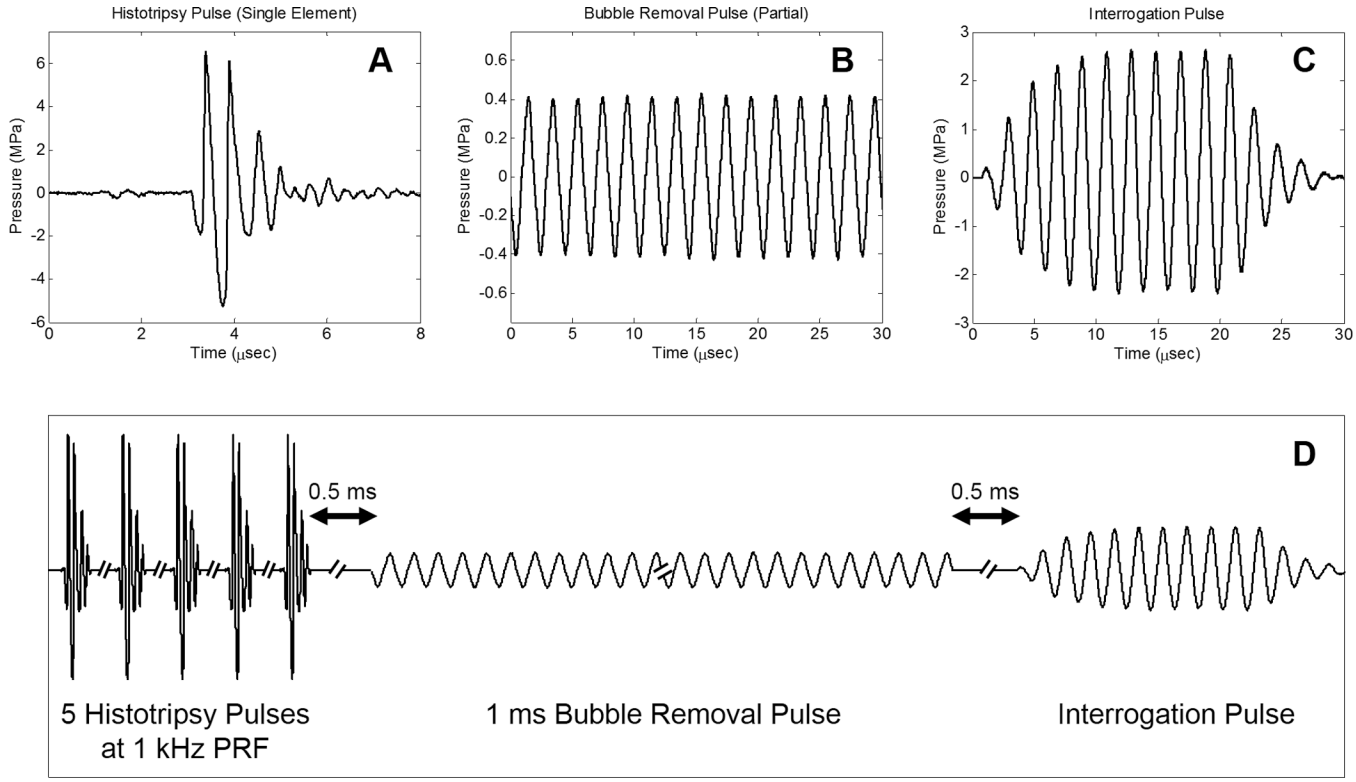

Fig. 2.

General pulse scheme used to study the effect of low-amplitude acoustic bursts on residual cavitation bubble nuclei. **A.** Representative waveform acquired from a single 2 MHz histotripsy module; the histotripsy pulse amplitude at the focal location can be estimated as the linear sum of the waveforms from all eight histotripsy modules, suggesting a focal peak negative pressure of approximately 40 MPa. **B.** Partial segment of the 1 ms bubble removal pulse; all bubble removal pulses had a center frequency of 500 kHz, while the amplitude was varied from 0 to 1.7 MPa. **C.** Interrogation pulse used to expand residual bubble nuclei remaining in the field; all interrogation pulses were generated by the 500 kHz bubble removal module, had duration of 10 cycles, and amplitude of 2.5 MPa. **D.** Overall timing of experimental pulse scheme. Further details can be found in the text.

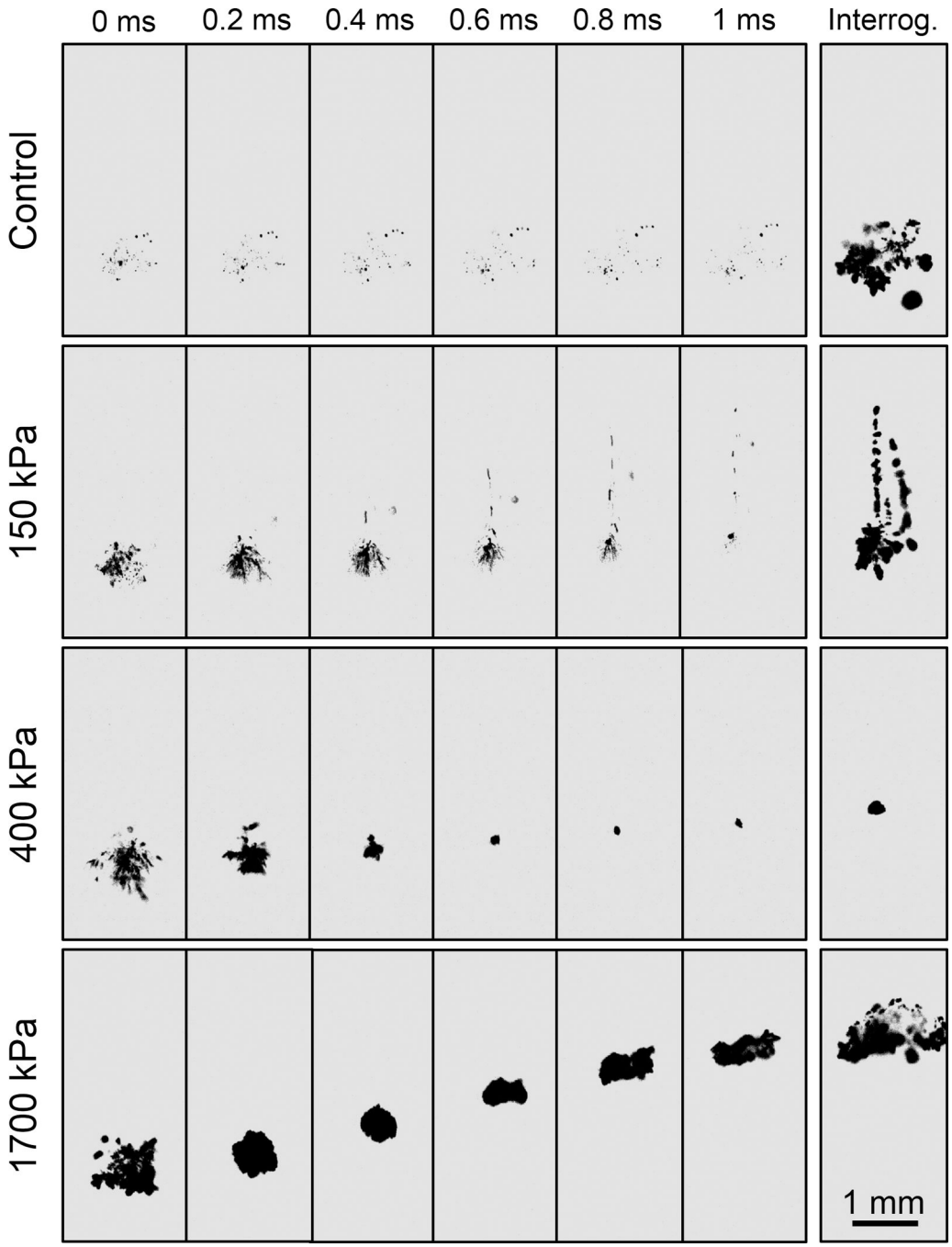

Fig. 3.

Representative backlit images of nuclei activity over the course of bubble removal and interrogation. Ultrasound propagates from bottom to top in each frame, and t= 0 ms corresponds to the arrival of the bubble removal pulse. Four distinct cases are presented, including bubble removal pulse amplitudes of 0 (control), 150, 400, and 1700 kPa. For each, the activity of residual bubble nuclei is displayed at 0.2 ms intervals over the duration of the 1 ms bubble removal pulse; the last frame in each row shows the result of the corresponding interrogation pulse. Optimal bubble nuclei coalescence occurred at intermediate bubble

removal pulse amplitudes (e.g. 400 kPa). At lower amplitudes (e.g. 150 kPa) minimal coalescence was observed, although some bubble dispersion was induced. At higher amplitudes (e.g. 1700 kPa) residual nuclei underwent violent cavitation, the collapse of which produced additional remnant daughter bubbles. This paper has supplementary downloadable material available at http://ieeexplore.ieee.org, provided by the authors. This includes the full video sequences corresponding to the image sets displayed in Fig. 3. All videos were taken at 20 kfps with a 49 μs exposure, and show the entire duration of the experimental pulse sequence displayed in Fig. 2.

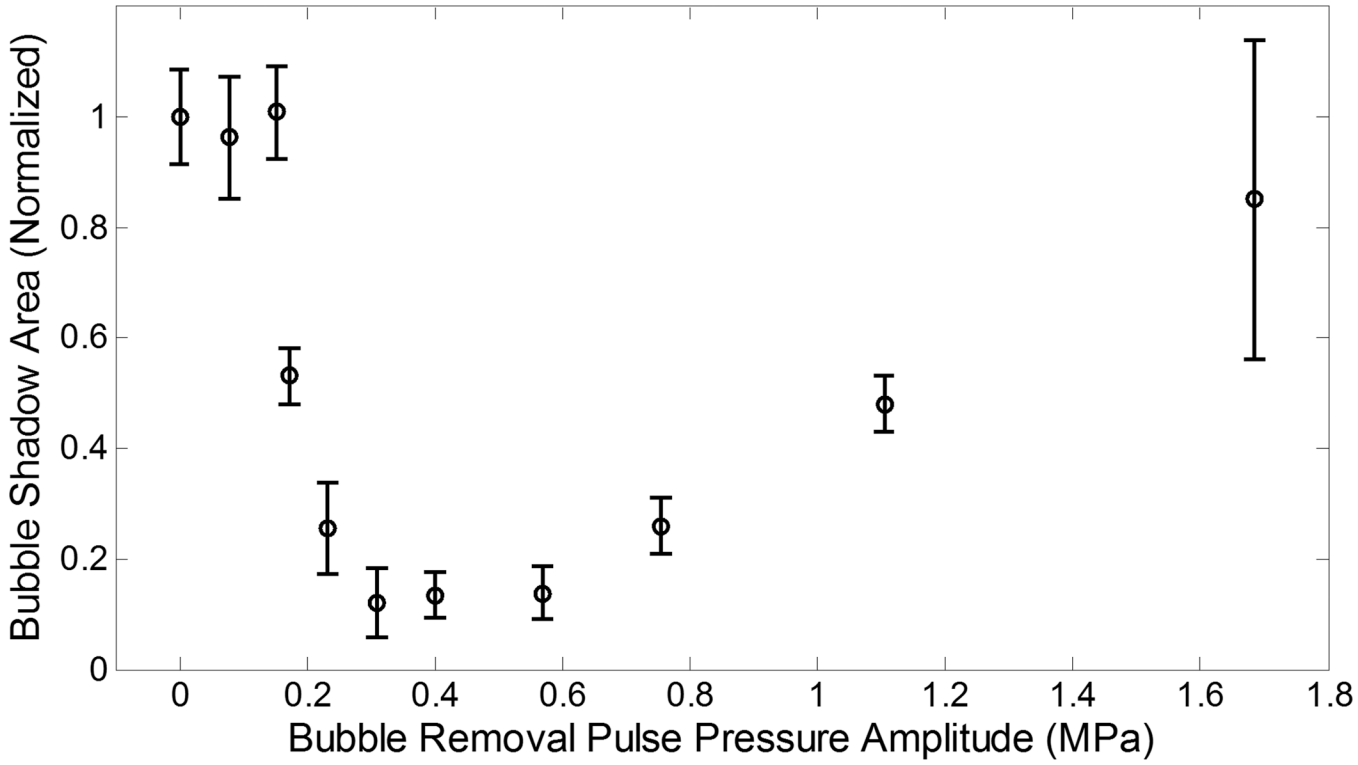

Fig. 4.

Backlit area of shadow (mean ± SD) from bubbles expanded by the interrogation pulse (normalized to the control case). Bubble removal pulses with amplitudes of 80, 150, and 1700 kPa did not produce a statistically significant change in interrogated bubble shadow area relative to control, while those with amplitudes ranging from 150 – 1100 kPa resulted in a statistically significant reduction. Within the later range, interrogated bubble shadow area was observed to decrease with increasing bubble removal pulse amplitude until reaching a minimum in the vicinity of 310 – 570 kPa. Further increase in bubble removal pulse amplitude resulted in an increase in interrogated bubble shadow area. These trends are correlated to observations from high speed photography in the text.